IJE TRANSACTIONS A: Basics Vol. 34, No. 7, (July 2021) 1750-1765

International Journal of Engineering

Journal Homepage: www.ije.ir

Stability Analysis of AC/DC Microgrids in Island Mode

M. Khanalizadeh Eini, M. Mirhosseini Moghaddam*, A. Tavakoli, B. Alizadeh

Department of Electrical Engineering, Lahijan Branch, Islamic Azad University, Lahijan, Iran

PAPER INFO

Paper history:
Received 14 April 2021
Received in revised form 08 May 2021
Accepted 22 May 2021

Keywords:
AC/DC Microgrid
Islanded Performance
Microgrid Stability
Nonlinear Controller

ABSTRACT

This study aims to introduce a new structure based on a nonlinear controller for controlling and analyzing the stability of the microgrids. In the proposed model, AC and DC resources and loads are located on two different sides. In addition, an AC/DC bidirectional interface converter is applied to supply loads by AC/DC sources. There are AC/DC products on both sides of the converter and each side can supply the load of the other side via a bidirectional interface converter and its load. Alternatively, an energy storage system is used for the system stability on the DC side. The nonlinear microgrid controller is designed to adjust the AC bus side frequency and the DC bus side voltage properly. In this structure, the coordinated optimal power exchange and precise regulation of control signals lead to constant improvement. Thus, system performance is improved. The results show that the proposed model is efficient for both reduction of the fluctuations and improvement of the system stability

***doi**: 10.5829/ije.2021.34.07a.20*

1. INTRODUCTION

A microgrid (MG) is a combined distributed generation unit (DG), load-bearing unit, and energy storage system operating as connect to the network, island, or transition between two modes. There are some advantages in applying microgrids such as enhancing the level of reliability and customer satisfaction, improvement of the power quality and voltage profile levels, also an increase level of the flexibility while minimizing the energy losses [1, 2]. The structure of existing microgrids is in the form of AC, DC, or combined AC/DC, where the advantages of both AC and DC microgrids in the combined structure are applied. Nevertheless, the growing trend of applying combined AC/DC microgrids has significantly led to increase sustainability problems in these interconnected structures. The problem of sustainability in microgrids is mainly due to the lack of energy resources in the islanded operation mode as well as the inertia required for responding to dynamic frequency variations in manufacturing units. Thus, maintaining stable performance in power changing conditions and occurrence of faults is considered a key issue in controlling microgrids [3, 4]. Accordingly, in order to maintain the system stability, proper control decisions should be made by the control system based on dynamic network changes. Hence, the main goal of the distribution system operator in using microgrids is optimal power-sharing in islanded mode and grid-on, frequency control, and stable operation in sudden power changes conditions as well as during fault occurrence [5]. Different methods have been proposed by Li et al. [6] and Dragičević et al. [7] to analyze and improve the stability of microgrids. These studies have mainly focused on improving control methods. Note that the structure of microgrid and its operational features are very different from those of traditional networks.

The studies related to microgrid stability have mainly focused on the mathematical model of microgrid stability analysis to improve its stability [8]. Microgrid stability is improved through optimizing droop benefits. The microgrid model affects the accuracy and speed of calculation. However, many studies have been conducted on the proposed models to improve the accuracy of microgrid stability analysis. When the load fluctuates, the DGs adjust their output power dynamically and participate in the voltage regulation as well as microgrid frequency. The system stability improvement is achieved

* Corresponding Author Institutional Email: m.mirhosseini@liau.ac.ir
(M. Mirhosseini Moghaddam)

Please cite this article as: M. Khanalizadeh Eini, M. Mirhosseini Moghaddam, A. Tavakoli, B. Alizadeh, Stability Analysis of AC/DC Microgrids in Island Mode, International Journal of Engineering, Transactions A: Basics Vol. 34, No. 7, (2021) 1750-1765

by adding a complementary control loop, creating three-level control, and other optimization methods [9, 10].

Nikos [11] has improved AC/DC hybrid microgrid controller method which was applied to model, control, and simulate the microgrid. Employing a linear droop controller such as voltage feedback led to increased microgrid voltage stability in the islanded mode. Note that numerous converters were employed and their fluctuations were considered. Dheer et al. [12] have introduced a method analogous to the normal droop control in which the feedback was taken from the phase angle instead of sampling the voltage magnitude, and the phasor area was analyzed. The DC side loads and resource had not been considered. Implementing this control method in the grid-on microgrids involving an AC/DC source resulted in more precision in the reactive power distribution to control the voltage. A hierarchical control method with three control levels was suggested by Khorsandi at al. [13], in which droop control was performed at the primary level. Then, the deviations generated in the primary controller were compensated at the secondary level and the load section was managed by the microgrid at the third level. Complex implementation could be considered a disadvantage of this method. A dynamic analysis of the DC link on the energy storage along with the generation resources was performed by Tejwani and Suthar [14]. In that model, the strategy of droop control was used for various operational modes, power distribution between units, and microgrid frequency control. Furthermore, in the storage source, there was a boost converter which would charge and recharge the battery. The droop values of the control loop were set at two levels in order to maintain the small-signal stability and allowable system frequency [15].

Additionally, optimization methods are used to determine droop values. Yu et al. [15] have presented a small signal stability model for voltage control and microgrid current. The equations were based on state-space equations. This model included nonlinear equations converted to a linear equation after simplification. Note that AC/DC coordination was not considered which barely affects the system efficiency. Thale and Agarwal [16] have analyzed the small-signal stability for two parallel inverters connected to a network-independent AC system. Analyzing the small-signal stability helps choose the optimal droop utility and the cutoff frequency of the system. However, it is hard to describe the dynamic behavior of connected parallel inverters which cannot be applied to every system.

In this research, a new structure based on a nonlinear controller is proposed to analyze the stability of microgrids in the presence of renewable energy sources as well as energy storage. Based on this model, several challenges of hybrid microgrids are solved. First, the hybrid microgrid is defined as two independent AC and DC buses. In this way, each bus prevents increase in the number of converters on each side by providing loads on its side. In addition, a bidirectional AC/DC interface converter is employed to connect these two buses, which is the criterion for power exchange between these buses through the interface converter of DC side voltage changes and AC side frequency changes. Meanwhile, independent nonlinear control for each element is defined based on the value of error relative to the reference value. As a result, eliminating the error of all system elements will lead to system stability. Finally, to improve the stability of the system, a suitable algorithm is used to charge and discharge energy storage resources. A battery and a capacitor bank are utilized to model the energy storage resources, which can act as system backups in different charging and discharging modes.

In the following, the dynamic modeling of PV and wind resources as well as energy storage is provided first. Then, the structure of the proposed model for accurate control and coordination of AC/DC sectors is described. Finally, the study system and simulation results are presented.

2. MODELING RESOURCES AND CONVERTERS

The model to be introduced involves production sources and AC/DC loads, and can connect to the network. Similar to solar cells (PVs), batteries, and direct winds, the DC resources connect to a DC link through their interface converter. Using this bus, they feed the loads that require the DC power. As with diesel generators, AC power supplies are connected to the AC bus, through which AC loads are also fed. The DC power generated in the DC bus may be transmitted to the AC bus by a bidirectional converter and vice versa. In the main model, all sources and converters are required to be dynamically modeled.

Figure 1 displays the diagram of the microgrid structure such as two AC and DC sections with interface converter. In such a system, changes in load or generation on one side can affect the other side. The power required to maintain the stability of the system is supplied through the same bus or the other side.

The controllers are designed in a decentralized model to generate their power according to the needs of each part, while stabilizing the DC voltage and AC frequency. The AC/DC hybrid microgrid consists of a PV unit with a DC/DC converter, a wind permanent magnet synchronous generator with an AC/DC converter. The energy storage system is connected to the DC bus via a DC/DC bidirectional converter. On the AC side, a synchronous generator is directly connected to the AC bus, and both buses are connected to each other by a bidirectional VSC converter with an LC filter. The dynamic model of resources and converters are described as follows.

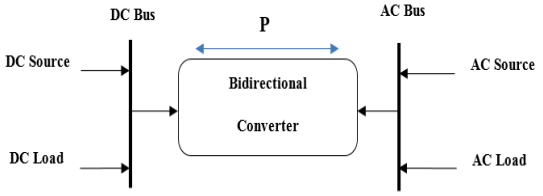

Figure 1. The diagram of AC/DC microgrid structure

2. 1. Modeling PV Power System in DC Microgrids The simulated PV energy system consists of a PV module and a boost converter [17]. Figure 2 reveals the diagram of the converter circuit. This system includes GBT switch, L inductance, Cpv input capacitor, D diode, and Cdc output capacitor. The converter is assumed to operate continuously in the steering mode.

$$\frac{dx_1}{dt}=\frac{1}{L}\left[-R\cdot x_1+x_2-(1-\mu_1)x_3\right] \quad (1)$$

$$\frac{dx_2}{dt}=\frac{I_{pv}-x_1}{C_{pv}} \quad (2)$$

$$\frac{dx_3}{dt}=\frac{1}{C_{dc}}\left[(1-\mu_1)x_1-i_o\right] \quad (3)$$

where, x_1, x_2, x_3, and μ_1 represent the PV current (i_L), mean values of input voltage (V_{pv}), PV output voltage (V_{opv}), and control signal (μ_1), respectively. C_{PV}, C_{dc}, L, I_{PV}, R, and i_o are the PV voltage stabilization capacitor, DC voltage stabilization capacitor, inductance, output current of PV cell, resistance, and output current of PV converter, respectively.

2. 2. Modeling the Wind Power System Figure 3 illustrates the wind power supply mechanism performed by a permanent magnetic synchronous generator. In this figure, an intermediate rectifier is used between the generator and the DC bus plus the boost converter. Since the output power changes according to the wind speed change, the output voltage should be adjusted to the desired level [18]:

$$\frac{dx_4}{dt}=\frac{V_{in}}{L_w}-\frac{R_w}{L_w}x_4-(1-\mu_2)\frac{x_5}{L_w} \quad (4)$$

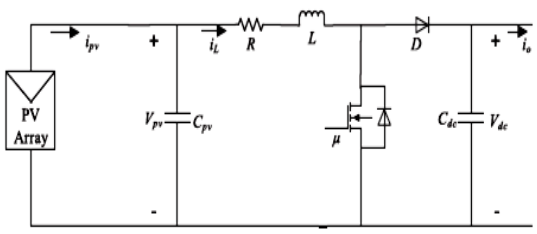

Figure 2. PV source converter circuit diagram

$$\frac{dx_5}{dt}=(1-\mu_2)\frac{x_4}{C_w}-\frac{I_{owind}}{C_w} \quad (5)$$

where, x_4, x_5, and μ_2 are the mean values of wind source current (i_w), wind source output voltage (V_w), and control signal (μ_2), respectively. I_{owind} and V_{in} denote the output current of the converter and voltage generated by the wind source, respectively. In addition, this model includes L_w input inductor with R_w series resistance, D diode (rectifier), C_w output capacitor, and IGBT switch.

2. 3. The Dynamic Models of Diesel Generator and Turbine's Controller In this paper, a two-axis model of the diesel generator is implemented. The dynamic model contains both mechanical and electrical dynamics. The excitation system is the main part of diesel generator where an excitation controller is used to maintain the terminal voltage at the desired level. The turbine control system adjusts the generator power output.

The complete dynamics model of the diesel generator with the presence of mechanical and electrical structures as well as the dynamics of the turbine and excitation system can be represented by the following equations [19]:

$$\frac{dx_6}{dt}=x_7+\omega_0 \quad (6)$$

$$\frac{dx_7}{dt}=-\frac{D}{2H}(x_7-\omega_0)+\frac{\omega_0}{2H}x_{11}-\frac{\omega_0}{2H}(x_8I_q+x_9I_d) \quad (7)$$

$$\frac{dx_8}{dt}=-\frac{1}{T'_{do}}x_8-\frac{(x_d-x'_d)}{T'_{do}}I_d+\frac{1}{T'_{do}}(x_{10}) \quad (8)$$

$$\frac{dx_9}{dt}=-\frac{1}{T'_{qo}}x_9+\frac{(x_q-x'_q)}{T'_{qo}}I_q \quad (9)$$

$$\frac{dx_{10}}{dt}=-\frac{x_{10}}{T_A}-\frac{K_A}{T_A}(V_{ref}+V_c-V_t) \quad (10)$$

Turbine's controller system:

$$\frac{dx_{11}}{dt}=-\frac{x_{11}}{T_T}+\frac{K_T}{T_T}x_{12} \quad (11)$$

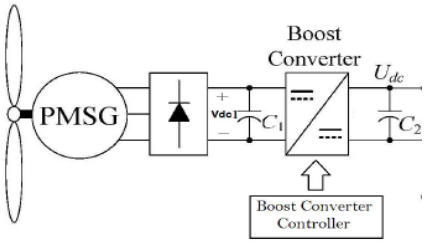

Figure 3. The diagram of wind circuit and its converter

$$\frac{dx_{12}}{dt} = -\frac{x_{12}}{T_G} + \frac{K_G}{T_G}P_C - \frac{K_G}{R_r\omega_0 T_G}x_7 \quad (12)$$

where, x_6, x_7, x_8, x_9, x_{10}, x_{11}, and x_{12} are the values of the angular load (δ), rotor velocity (ω), leakage flux field variable of q axis (E_q), leakage flux variable of d axis (E_d), excitation field voltage (E_{fd}), mechanical power (P_m), and reactance distribution (X_m). In addition, other parameters have their usual definitions as discussed by Abdullah et al. [19].

2. 4. Modeling the Combined Energy Storage System The storage device connected to the DC bus is shown in Figure 4. The combined system includes a battery and a capacitor bank. The battery connects to the DC bus through a boost-buck converter, consisting of an inductor, Rbat series resistor, output filter capacitor, and two IGBT switches [1]. Both switches are controlled through their signal. The converter is used to adjust the DC bus voltage. It can operate in a charge and discharge mode depending on the load demand. Further, the capacitor bank (CB) is connected to the DC bus through the boost converter. These two states are expressed mathematically as follows.

$$Z = \begin{Bmatrix} 1, & if\ (i_{batref} > 0) \\ 0, & if\ (i_{batref} < 0) \end{Bmatrix}, Y = \begin{Bmatrix} 1, & if\ (i_{bcref} > 0) \\ 0, & if\ (i_{bcref} < 0) \end{Bmatrix} \quad (13)$$

where, i_{batref} is the battery's reference current generated through controlling its level based on electricity demand. If $i_{batref} > 0$ and $i_{bc} > 0$, then the battery converter is modeled by the following differential equations:

$$\begin{aligned} \frac{di_{bat}}{dt} &= \frac{V_{bat}}{L_{bat}} - \frac{R_{bat}}{L_{bat}}i_{bat} - (1-\mu_3)\frac{V_{dc}}{L_{bat}} \\ \frac{di_{CB}}{dt} &= \frac{V_{CB}}{L_{CB}} - \frac{R_{CB}}{L_{CB}}i_{CB} - (1-\mu_5)\frac{V_{dc}}{L_{CB}} \end{aligned} \quad (14)$$

where, i_{bat}, i_{CB}, μ, V_{bat}, and V_{dc} represent the battery output current, capacitor bank output current, control signal, battery voltage, and DC bus voltage, respectively. In addition, R_{bat}, L_{bat}, and C_{dc}, are the series resistance with battery source, the inductor series with battery source, the converter output capacitor. If $i_{batref} < 0$ and $i_{CBref} < 0$, then the differential equations are stated as follows:

$$\begin{aligned} \frac{di_{bat}}{dt} &= \frac{V_{bat}}{L_{bat}} - \frac{R_{bat}}{L_{bat}}i_{bat} - (\mu_4)\frac{V_{dc}}{L_{bat}} \\ \frac{di_{CB}}{dt} &= \frac{V_{CB}}{L_{CB}} - \frac{R_{CB}}{L_{CB}}i_{CB} - (\mu_6)\frac{V_{dc}}{L_{CB}} \end{aligned} \quad (15)$$

In order to simplify the system, a virtual control signal is introduced as follows:

$$\begin{aligned} \mu_{Bat} &= [K - (1-\mu_3) + (1-K)\mu_4] \\ \mu_{CB} &= \left[L(1-\mu_5) + (1-L)\mu_6\right] \end{aligned} \quad (16)$$

Finally, Equations (14), (15), and (16) lead to the following equations.

$$\frac{dx_{13}}{dt} = \frac{V_{bat}}{L_{bat}} - \frac{R_{bat}}{L_{bat}}x_{13} - \mu_{Bat}\frac{x_3}{L_{bat}} \quad (17)$$

$$\frac{dx_{14}}{dt} = \frac{V_{CB}}{L_{CB}} - \frac{R_{CB}}{L_{CB}}x_{14} - \mu_{CB}\frac{x_3}{L_{CB}} \quad (18)$$

where, x_{13} and x_{14} denote the mean values of (i_{bat}) battery current and the capacitor bank current (i_{CB}), while μ_{Bat} and μ_{CB} are the mean values of control signals.

2. 5. Bidirectional Converter Model of DC Bus Interface, AC Bus, and Filter The interface converter between AC and DC sections should have both rectifier and inverter capabilities. If the output power of the AC side is less than its power consumption, it would be necessary to receive part of the required power through the DC side. In this case, the converter acts as an inverter. Also, if the output power of the DC side is low, it is necessary to receive part of the required power through the AC side. In this case, the converter functions as a rectifier. The converter receives the changes according to DC voltage and AC voltage as well as frequency and acts accordingly. The following equations indicate the relationships between the various variables of the system [20, 21].

$$\begin{aligned} \frac{dx_{15}}{dt} &= -\frac{R}{L}x_{15} + x_7 x_{16} + u_{d1} \\ \frac{dx_{18}}{dt} &= -\frac{R}{L}x_{18} + x_7 x_{19} + u_{d2} \end{aligned} \quad (19)$$

$$\begin{aligned} \frac{dx_{16}}{dt} &= -x_7 x_{15} - \frac{R}{L}x_{16} - u_{q1} \\ \frac{dx_{19}}{dt} &= -\frac{R}{L}x_{19} - x_7 x_{18} + u_{q2} \end{aligned} \quad (20)$$

$$\begin{aligned} \frac{dx_{17}}{dt} &= \frac{3u_{sq1}x_{16}}{2C\,x_{17}} - \frac{i_L}{C} \\ \frac{dx_{20}}{dt} &= \frac{3u_{sq2}x_{19}}{2C\,x_{20}} + \frac{i_L}{C} \end{aligned} \quad (21)$$

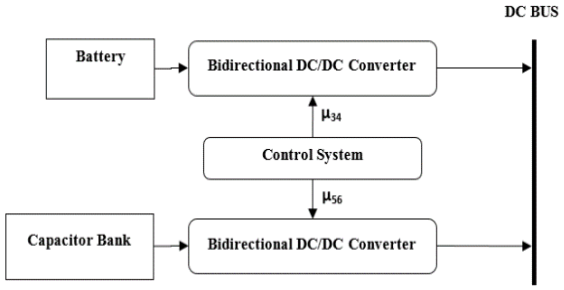

Figure 4. Combined storage system model and control algorithm

where, u_{sd1}, u_{sd2}, u_{sq1}, and u_{sq2} are the components of the d and q axes of the source voltage related to both rectifier and inverter modes, respectively. Further, x_{15}, x_{16}, x_{18}, and x_{19} are the line current components while u_{rd1}, u_{rd2}, u_{rq1}, and u_{rq2} are the input voltage components of the converter in both inverter and rectifier modes.

3. NONLINEAR CONTROL METHOD

The backstepping nonlinear control method is developed based on the dynamic model of each microgrid component. PV, wind, energy storage, and synchronous generator resources along with the corresponding converter are controlled by their respective control system. The most important part of this model is the bidirectional converter. This converter is controlled through the signals of voltage and frequency on both sides. The control method for each section is shown in Figure 5. In this model, the resources are controlled based on backstepping method. Each production source and interface converter will be controlled independently. Specifically, the sum of the error of each unit becomes zero. The error of each unit independently tends to zero. Hence, the derivative of the sum of Lyapunov's functions also tends to be zero. In this way, both the error of each unit and the error of the entire system are zero. This indicates the stability of the system whereby the system will be practically stable. The main role of stability is played by the control variable. Each unit generates a control signal that always sets the system error to zero. To prove the equation of the control variable, the derivative of the Lyapunov energy function is set to zero where the equation of the control variable is obtained. Next, initially, the error of each unit is compared with its reference value after which it is solved using the backstepping method.

In this method, the error of each unit is measured first and then compared with the base value. Thereafter, via the backstepping method, the system output is stabilized by the control and input changes. In the proposed model, the sources are controlled independently and by their own error. Practically, the main criterion is the voltage of DC bus as well as voltage and frequency of the AC bus. The value of error in each unit is measured by its own control system, which tends to zero. It can be stated that the total errors of the entire system will be equal to zero. The design method is summarized as follows:

1) Calculating the errors for each control target or state variable.
2) Calculating the dynamics of the error.
3) Calculating Lyapunov function and its derivatives based on errors.
4) Repeating the first three steps until the control rules appear.
5) Calculating control rules to stabilize the error dynamics in the last step.
6) Stability analysis of the entire system with the derived control rules.

Load supply is the most important issue in hybrid microgrids. Voltage changes are a good operational indicator for controlling load changes in DC bus. To evaluate these changes, the power balance on the DC side must first be checked. Accordingly, the amount of net power (P_{net}) in the microgrid can be defined as follows:

$$P_{net} = P_w + P_{pv} + P_{ESS} - P_{loss} - P_{load,DC} \pm P_{transfer} \quad (22)$$

P_{pv}, P_w, and P_{ESS} are the output power of PV, wind source, and storage system, respectively, $P_{Load,DC}$ is the power required for the DC side load, $P_{transfer}$ denotes the power exchanged between the AC and DC bus, and P_{loss} reflects the system loss. Under these circumstances, P_{ESS} plays an important role in maintaining the microgrid stability. The dynamics of the DC bus voltage in a microgrid can be adjusted based on the following principle of power balance:

$$CV_{dc}\frac{dV_{dc}}{dt} = P_{net} \ , \ P_{DC,TOT} = V_{dc} i_{dc,TOT} \quad (23)$$

where, V_{dc} , $i_{dc,ToT}$, and $P_{dc,ToT}$ represent DC bus voltage, sum of the current injected into the DC bus by the sources, and the sum of DC power, respectively. C capacitance is equivalent to the output for all converters. From the above equation, it can be seen that the DC bus voltage depends on the power balance in this bus and the elevation or reduction of DC bus voltage indicates excess or lack of power. To adjust the DC bus voltage, the power balance in the DC bus must be maintained. PV, wind, and storage sources first receive the error relative to the reference value and then generate a proportional control signal to compensate for this error. If the DC side sources cannot respond to the load increase, the power required from the AC side is provided by a bidirectional interface converter.

3. 1. PV Control The main goal is to control the DC output voltage of the DC-DC converter by changing the duty cycle in relation to the solar radiation variations. First, the error equation of each state variable is calculated with respect to the reference value. The design method of PV control scheme and connected converter goes through the following steps:
Step 1: Depending on the purpose of the design, the first tracking errors are defined as follows:

$$e_1 = x_2 - V_{PV(ref)} \quad (24)$$

The dynamics of e_1 is as follows:

$$\frac{de_1}{dt} = \frac{1}{C_{PV}}\left(i_{PV} - x_1\right) - \frac{dV_{PV(ref)}}{dt} \quad (25)$$

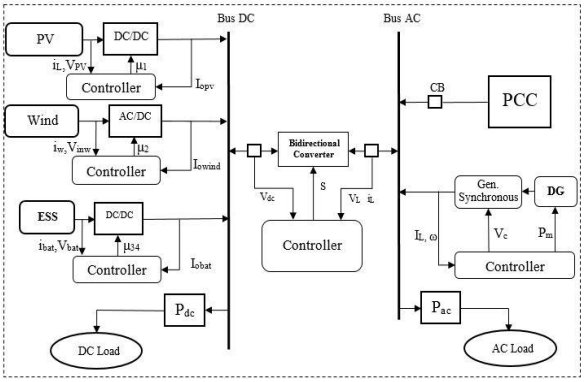

Figure 5. The control system model

where, x_1 is a stabilizing function, for which the Lyapunov function is:

$$V_1 = \frac{1}{2}e_1^2 \tag{26}$$

Incorporating Equation (25) into Equation (26) yields:

$$\frac{dV_1}{dt} = e_1\left(\frac{1}{C_{PV}}\left(i_{PV} - x_1\right) - \frac{dV_{PV\,(ref)}}{dt}\right) \tag{27}$$

To ensure the dynamic stability the derivative of e_1, the derivative of V_1 should be a definite or semi-definite negative. To achieve this, the system parameters are set as follows:

$$\frac{1}{C_{PV}}\left(i_{PV} - x_1\right) - \frac{dV_{PV\,(ref)}}{dt} = -c_1 e_1 \tag{28}$$

Where, c_1 is used to set the output response. Embedding Equation (28) into Equation (27) yields:

$$\frac{dV_1}{dt} = -c_1 e_1^2 \le 0 \tag{29}$$

The combined value α of i_L can be determined from Equation (29) as follows:

$$\alpha = C_{PV}\left(\frac{dV_{PV(ref)}}{dt} - c_1 e_1\right) - i_{PV} \tag{30}$$

Step 2: To achieve zero tracking error, the i_L inductor current should be equal to α. Hence, another error variable is defined as follows:

$$e_2 = x_1 - \alpha \tag{31}$$

Derivation of Equation (31) leads to the dynamics of the error as follows:

$$\frac{de_2}{dt} = \frac{1}{L}\left(-Rx_1 + x_2 - \left(1-\mu_1\right)x_3\right) - \frac{d\alpha}{dt} \tag{32}$$

In this case, Lyapunov second function is equal to:

$$V_2 = V_1 + \frac{1}{2}e_2^2 \tag{33}$$

its derivative is:

$$\frac{dV_2}{dt} = -c_1 e_1^2 + c_2\frac{de_2}{dt} \tag{34}$$

The stability of the dynamic error (derivative of e_2) is obtained only if the derivative of V_2 is less than or equal to zero. Hence,

$$\frac{de_2}{dt} = \frac{1}{L}\left(-Rx_1 + x_2 - \left(1-\mu_1\right)x_3\right) - \frac{d\alpha}{dt} = -c_2 e_2 \tag{35}$$

Using Equations (34) and (35), the main function is determined as follows:

$$\frac{dV_2}{dt} = -c_1 e_1^2 + c_2 e_2^2 \le 0 \tag{36}$$

Which is a definite or semi-definite negative. The proposed control law, along with the sustainability analysis of the entire PV system, is shown in the next step.

Step 3: Since the condition shown by Equation (35) is not correct, it is necessary to analyze the overall stability of the system. For this purpose, the final error based on Equation (36) is defined as follows:

$$e_3 = \frac{1}{L}\left(-Rx_1 + x_2 - \left(1-\mu_1\right)x_3\right) - \frac{d\alpha}{dt} + c_2 e_2 \tag{37}$$

The dynamics of which is written as follows:

$$\frac{de_3}{dt} = \frac{1}{L}\begin{pmatrix} -R\dfrac{dx_1}{dt} + \dfrac{dx_2}{dt} + \dfrac{d\mu_1}{dt}x_3 \\ -\left(1-\mu_1\right)\dfrac{dx_3}{dt} \end{pmatrix} - \frac{d^2\alpha}{dt^2} + c_2\frac{de_2}{dt} \tag{38}$$

At this stage, Lyapunov function is presented as follows:

$$V_3 = V_2 + \frac{1}{2}e_3^2 \tag{39}$$

By substituting the derivative of V_2 of Equation (36) and $\dot{e}_3$ of Equation (38) in Equation (39), the derivative V_3 is stated as follows:

$$\frac{dV_3}{dt} = c_3 e_3\begin{pmatrix} \dfrac{1}{L}\begin{pmatrix} -R\dfrac{dx_1}{dt} + \dfrac{dx_2}{dt} \\ +\dfrac{d\mu_1}{dt}x_3 - \left(1-\mu_1\right)\dfrac{dx_1}{dt} \end{pmatrix} \\ -\dfrac{d^2\alpha}{dt^2} + c_2\dfrac{de_2}{dt} \end{pmatrix} - c_1 e_1^2 - c_2 e_2^2 \tag{40}$$

Now, the final control law is selected as follows:

$$\frac{d\mu_1}{dt}=-\frac{1}{x_3}\left(\begin{array}{l}\frac{1}{L}\left(\begin{array}{l}-R\frac{dx_1}{dt}+\frac{dx_2}{dt}+\frac{d\mu_1}{dt}x_3\\-(1-\mu_1)\frac{dx_3}{dt}\end{array}\right)\\-\frac{d^2\alpha}{dt^2}+c_2\frac{de_2}{dt}+c_2e_2\end{array}\right) \tag{41}$$

where, $0<\mu_1<1$, then the presented control law is used to generate the duty cycle of the PV converter. Similar steps are used to obtain control rules for the bidirectional DC/DC converter of the storage system plus the excitation system of synchronous generators. Accordingly, the derivative of these control laws is discussed in the following sections without repeating these steps.

3. 2. DC/DC Converter Control for Wind Energy Integration The tracking error for the wind converter is expressed as follows:

$$e_4=x_4-I_{ref} \tag{42}$$

$$e_5=x_5-\sigma \tag{43}$$

The first function of the Lyapunov V_4 is selected to analyze the stability of the system as follows:

$$V_4=\frac{1}{2}e_4^2 \tag{44}$$

The derivative of V_4 should be semi-definite for the system to be completely stable ($V_4\leq 0$). To ensure the uninterrupted stability of the wind power system, the second combined set of V_5 sets is written as follows:

$$V_5=V_4+\frac{1}{2}e_5^2 \tag{45}$$

By taking the derivative V_5 and substituting the value V_4 of Equation (41), we have:

$$\frac{dV_5}{dt}=-c_4e_4^2+e_5\left(\frac{de_5}{dt}+\frac{(1-\mu_2)e_4}{L_w}\right) \tag{46}$$

Substituting e_5 of Equation (43) into Equation (46), we have:

$$\begin{aligned}\frac{dV_5}{dt}=&-c_4e_4^2+e_5\left(\frac{(1-\mu_2)x_4}{C_w}\right)\\&+e_5\left(-\frac{1}{(1-\mu_2)}-\frac{I_{owind}}{C_w}\right)\\&+e_5\left(-c_5e_5-\frac{\sigma}{(1-\mu_2)}\cdot\frac{d\mu_2}{dt}+\frac{(1-\mu_2)e_4}{L_w}\right)\end{aligned} \tag{47}$$

To keep the wind system dynamics constant, V_5 should run as follows:

$$\frac{dV_5}{dt}=-c_4e_4^2+c_5e_5^2 \tag{48}$$

$$\sigma=\frac{L_w}{(1-\mu_2)}\left(c_4e_4+\frac{V_{in}}{L_w}-\frac{dI_{ref}}{dt}-\frac{R_w}{L_w}x_4\right) \tag{49}$$

where $c_4>0$ and $c_5>0$ are the constant parameters. The control signal for μ_2 is obtained as follows:

$$\begin{aligned}\frac{d\mu_2}{dt}=&\frac{1}{\sigma}\left(\frac{e_4(1-\mu_2^2)}{L_w}\right)\\&+\frac{1}{\sigma}\left(-e_5(c_4-c_5)(1-\mu_2)+\frac{(1-\mu_2)^2x_4}{C_w}\right)\\&+\frac{1}{\sigma}\left(-\frac{(1-\mu_2)I_{owind}}{C_w}\right)\end{aligned} \tag{50}$$

where, $0<\mu_2<1$. Then the presented control law is employed to generate the time cycle of the wind turbine energy converter. The stability control system ensures asymptotic stability and convergence of error dynamic to zero.

3. 3. Controlling DC/DC Converters for Storage Source The control process of the storage source is presented as follows: 1. Adjusting the direct current bus voltage of the microgrid under the variations of load demand, 2. Tracking battery's fast current and capacitor bank current to their reference values, 3. Analyzing the asymptotic stability of the storage resource.

It is not possible to directly track the V_{dc} voltage from the V_{dcref} value. Thus, the indirect voltage regulation method is used to achieve this goal where I_{bat} is tracked by its reference value, obtained as follows:

$$I_{batref}=\left(\frac{V_{dcref}x_{13}-V_{CB}I_{CBref}}{\Phi V_{bat}}\right) \tag{51}$$

where, Φ represents the switching losses coefficient in the converters whose value should be greater than 1. To achieve control goals, the tracking error is defined as follows:

$$e_6=x_{13}-I_{batref}\ ,\ e_7=\frac{x_{13}}{L_{bat}}-\beta_0 \tag{52}$$

The chosen Lyapunov functions, V_6 and V_7, for analyzing the stability of the system are as follows:

$$V_6=\frac{1}{2}e_6^2\ ,\ V_7=V_6+\frac{1}{2}e_7^2 \tag{53}$$

The virtual control β_0 should be written as follows:

$$\beta_0=\frac{1}{\mu_{bat}}\left(c_5e_6+\frac{V_{bat}}{L_{bat}}-\frac{R_{bat}}{L_{bat}}x_{13}-\frac{dI_{batref}}{dt}\right) \tag{54}$$

The μ_{Bat} control law is defined as follows:

$$\frac{d\mu_{Bat}}{dt}=\frac{1}{\beta_0}\left[e_7\mu_{Bat}^2-\mu_{Bat}^2\frac{R_{bat}}{x_{13}C_{dc}}-\mu_{Bat}\frac{R_{bat}}{C_{dc}}\right]+\frac{1}{\beta_0}\left[\mu_{Bat}\frac{x_{13}}{L_{bat}C_{dc}}-\mu_{Bat}c_6e_6\right] \quad (55)$$

Similarly, the signal control converter is obtained in the capacitive bank system as follows:

$$\frac{d\mu_{CB}}{dt}=\frac{L_{CB}}{x_{14}}\left(\frac{V_{CB}}{L_{CB}}-\frac{R_{CB}}{L_{CB}}x_{14}-c_7e_7-\frac{dI_{CBref}}{dt}\right) \quad (56)$$

Where, $0<\mu_{Bat}<1$ and $0<\mu_{CB}<1$ represent the control law used to create a time cycle for the bidirectional converter connected to the battery. $\beta_0\neq0$ and $c_{6\&7}>0$ are the gain of controller in the controller design, and the μ_{CB} is employed to generate a time cycle of the bidirectional converter connected to the capacitor bank.

3. 4 Excitation Control and Backstepping Valve Steam for Synchronous Generator Applying the proposed backstepping control scheme can contribute to control the excitation system and steam valve. The chosen Lyapunov function, V_8, for analyzing the stability of the system is as follows:

$$V_8=\frac{1}{2}e_8^2 \quad (57)$$

The excitation control input is defined as:

$$V_c=\frac{x_{10}}{K_A}-(V_{ref}-V_t)+\frac{T_A}{K_A}\cdot\frac{d\beta_5}{dt}-\frac{T_A}{K_A}c_8e_8 \quad (58)$$

Also, the steam valve position control input is:

$$P_c=-\frac{T_G}{K_G}\left(-\frac{x_{12}}{T_G}+\frac{K_Gx_7}{R_r\omega_0T_G}-\frac{d\beta_6}{dt}+c_8e_9\right) \quad (59)$$

where:

$$\beta_1=-c_7e_8\ ,\ \beta_2=\frac{T_T}{K_T}\left(\frac{x_{11}}{T_T}-e_8c_8\right),$$

$$\beta_3=\frac{x_{11}}{I_q}-\frac{D}{I_q\omega_0}(x_7-\omega_0)+\frac{2H}{I_q\omega_0}(x_7-\omega_0)+\frac{2H}{I_q\omega_0}\cdot\frac{d\beta_1}{dt},$$

$$\beta_4=\frac{2H}{I_q\omega_0}c_8e_8$$

$$\beta_5=x_8+(x_d-x_d')I_d+T_{do}'\beta_3-T_{do}'c_8e_8\ ,$$

$$\beta_6=\frac{x_{11}}{I_q}-\frac{D}{I_q\omega_0}(x_6-\omega_0)+\frac{2H}{I_q\omega_0}(x_6-\omega_0)+\frac{2H}{I_q\omega_0}\cdot\frac{d\beta_1}{dt}$$

where, c_1-c_8 are positive constant parameters and e_1-e_8 are error variables.

3. 5. Bidirectional Converter Control between Two Sides If the output power of the DC side is less than its power consumption, it is necessary to receive part of the required power through the AC side. In this case, the converter acts as a rectifier. There are two controlled variables: i_{abc} and V_{DC}. Based on Equations (19)-(21), a controlling mathematical model can be expressed. First, the equations for the rectifier mode are described as below:

$$\frac{dx_r}{dt}=f_r(x)+g_ru_r,\quad y=h(x) \quad (60)$$

where, x is the rectifier state vector, u_r denotes the rectifier control input vector, y represents the rectifier output vector, while f and g are smooth vector fields.

$$X_r=\begin{bmatrix}x_{15}\\x_{16}\\x_{17}\end{bmatrix},f_r(x)=\begin{bmatrix}f_{r1}\\f_{r2}\\f_{r3}\end{bmatrix}=\begin{bmatrix}-\frac{R}{L}x_{15}+x_7x_{16}\\-x_7x_{15}-\frac{R}{L}x_{16}\\\frac{u_{sq1}x_{16}}{2Cx_{17}}-\frac{i_1}{C}\end{bmatrix},$$

$$g_r=\begin{bmatrix}\frac{1}{L}&0\\0&\frac{1}{L}\\0&0\end{bmatrix},\ u_r=\begin{bmatrix}u_{r1}\\u_{r2}\end{bmatrix}=\begin{bmatrix}u_{sd1}-u_{rd1}\\u_{sq1}-u_{rq1}\end{bmatrix} \quad (61)$$

The system has two control inputs in this case. Since some variables affect the system performance directly, it is better to use their effects for the feedback control law. The chosen Lyapunov function, V_9, for analyzing the stability of the system is as follows.

$$V_9=\frac{1}{2}e_9^2 \quad (62)$$

Hence, the output is chosen as:

$$y_1=i_{d1}\ ,\ y_2=v_{dc1} \quad (63)$$

The differential equations as well as the inputs and outputs are obtained based on Equations (60) and (62). The direct relationship between the inputs and outputs is easily obtained as below:

$$\begin{bmatrix}\frac{dy_1}{dt}\\\frac{d^2y_2}{dt^2}\end{bmatrix}=B_r+A_r\begin{bmatrix}u_{r1}\\u_{r2}\end{bmatrix} \quad (64)$$

$$B_r=\begin{bmatrix}f_{r1}\\\frac{3u_{sq1}}{2Cx_{17}^2}f_{r2}-\frac{3u_{sq1}x_{16}}{2Cx_{17}^2}f_{r3}-\frac{i_L}{C}\end{bmatrix},$$

$$A_r=\begin{bmatrix}\frac{1}{L}&0\\0&\frac{3u_{sq1}}{2CLx_{17}}\end{bmatrix}. \quad (65)$$

If the AC side output power is less than its power consumption, it is necessary to receive part of the required power through the AC side. In this case, the converter acts as an inverter. Thus, its state-space equations are of the second-order and with two inputs.

$$\frac{dx_i}{dt} = f_i(x) + g_i u_i, \tag{66}$$

Here we have:

$$X_i = \begin{bmatrix} x_{18} \\ x_{19} \end{bmatrix}, \quad f_i(x) = \begin{bmatrix} f_{i1} \\ f_{i2} \end{bmatrix} = \begin{bmatrix} -\frac{R}{L}x_{18} + x_7 x_{19} \\ -x_7 x_{18} - \frac{R}{L}x_{19} \end{bmatrix},$$
$$g_r = \begin{bmatrix} \frac{1}{L} & 0 \\ 0 & \frac{1}{L} \\ 0 & 0 \end{bmatrix}, \quad u_i = \begin{bmatrix} u_{i1} \\ u_{i2} \end{bmatrix} = \begin{bmatrix} u_{sd2} - u_{rd2} \\ u_{sq2} - u_{rq2} \end{bmatrix}, \tag{67}$$

where, u_{sd2}, u_{sq2}, u_{rd2}, u_{rq2}, i_{d2}, and i_{q2} denote the inverter state electrical parameters. Then, the output is chosen as:

$$w_1 = i_{d2}, \quad w_2 = i_{q2}. \tag{68}$$

Control inputs are displayed as follows:

$$\begin{bmatrix} u_{i1} \\ u_{i2} \end{bmatrix} = \begin{bmatrix} w_{1ref} - k_{13}e_{i1} - k_{32}\int e_{i1}dt \\ w_{2ref} - k_{41}e_{i2} - k_{42}\int e_{i2}dt \end{bmatrix} \tag{69}$$

Figure 6 indicates the nonlinear design diagram of the bidirectional converter.

3. 7. Stability Analysis The stability of a system refers to the system's ability to return back to its steady state after disturbance. The stability of isolated hybrid microgrids has been of major concern in electrical distribution systems. The stability of isolated hybrid microgrids determines whether the generation system can settle down to a new or original steady state once transients disappear. The stability of the distributed generation system depends on the loading and sudden changes in load which can cause the instability. Resources are controlled independently by their own error. The value of error in each unit is measured by its own control system, which tends to zero. Thus, practically the sum of the errors of the entire system will be equal to zero. In order to analyze the stability of a hybrid microgrid, the total energy functions of the system must be examined. These functions are as follows:

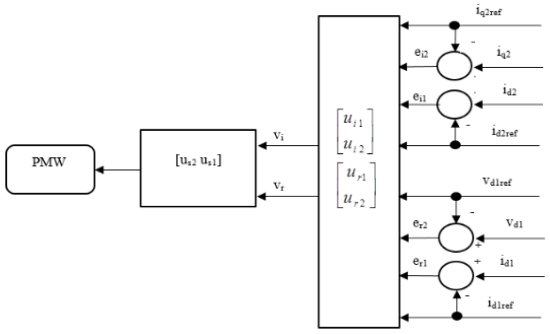

Figure 6. Nonlinear design diagram of the bidirectional converter

$$V_{total} = V_3 + V_5 + V_7 + V_8 + V_9 + e_8c_8 + e_9c_9 + (k_{31} + k_{32})e_{10} + (k_{41} + k_{42})e_{11} \tag{70}$$

$$\dot{V}_{total} = \dot{V}_3 + \dot{V}_5 + \dot{V}_7 + \dot{V}_8 + \dot{V}_9 + \dot{e}_8c_8 + \dot{e}_9c_9 + (k_{31} + k_{32})\dot{e}_{10} + (k_{41} + k_{42})\dot{e}_{11} \le 0 \tag{71}$$

The V_{total} must be negative semi-definite, which is calculated as below:
It can be observed that above equation is negative semi-definite. Thus, the stability of the entire hybrid microgrid system can be guaranteed. In other words, in cause of occurrence of a disturbance, the system will remain stable after the transition.

4. POWER CONTROL ALGORITHM

Power division or control between both sides is considered as the most important issue in AC/DC combined microgrids. Indeed, all resources, load, and bidirectional interface converters between both areas should be involved in this management. It is first assumed that resources, loads, and converters are controlled in a decentralized manner. Thus, a system is practically required to distribute the power. Then, if there is not enough generation on one side, the power should be compensated on the other side, and if the system power is not sufficient, the load must be cut off or reduced. Figure 7 depicts the power control algorithm. This algorithm is compatible with power converters connected to power resources by providing reference signals. The power equation in such a system is defined as below:

$$P_w + P_{pv} - P_{loss} = P_{load} + P_{ESS} \pm P_{transfer} \tag{72}$$

where, P_W, P_{pv}, P_{loss}, P_{load}, P_{ESS}, and $P_{transfer}$ are the wind power, PV power, power loss, load power, energy storage resource power, and diesel generator power, respectively.

Note that load changes on the AC side are practically modelled according to the power transmitted from or to the DC. The resources use a battery and a capacitor bank that can charge and discharge as well as support part of the system in different modes. Thus, both resources are employed to boost stability and provide an algorithm to control power. The predicted modes are as follows:

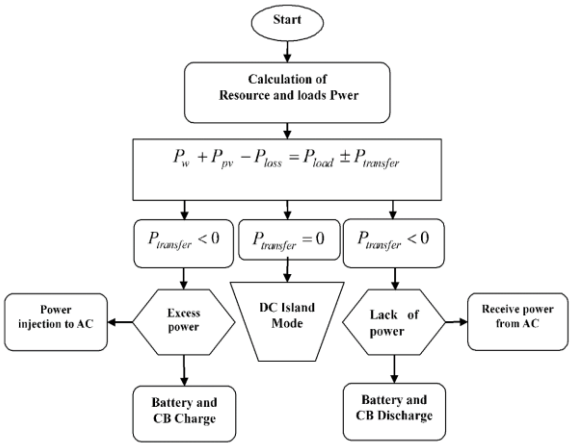

Figure 7. Energy management algorithm

1. The power in DC is surplus.
2. The power in DC is not enough to supply the load.
3. When the DC system gets disconnected due to fault.

In the first mode, the power generated by the resources on DC is greater than that of the load required in this sector. Hence, the surplus power is spent on recharging the energy source. The equations on DC are as follows.

$$P_{transfer} = P_{load} - \left(P_w + P_{pv} - P_{loss}\right) < 0$$
$$P_w + P_{pv} - P_{loss} = P_{load} \pm P_{transfer} \quad (73)$$

$P_{transfer}$ is the power given or taken from the AC. If it is negative, it means the power in DC is surplus. In this mode, both the distributed resources of generation and the energy storage system will share the load demand. The surplus power is utilized to charge the energy storage source or is sent to the other side. The battery does not change until it reaches 80%. In the second mode, the power generated by the resources on DC is less than the power required by the load in this section. Thus, there is a power shortage on this side, which should be supplied through an energy storage source from AC. The condition for power supply by the storage source is that it should be charged. The minimum charging capacity for power injection is 20%. The equations on DC are as follows.

$$P_{transfer\,2} = P_{load} - \left(P_w + P_{pv} - P_{loss}\right) > 0 \quad (74)$$

In the third mode, AC is separated from DC due to a fault or repair. In this case, there is no exchanging power. Thus, the DC system should supply the power required for this side. If the power is not sufficient to supply the load, the storage system will supply at least 20% of the load capacity if it is charged; otherwise, the load should be cut off. If the power is surplus, the storage system can start the charging process for optimal use of the energy, where charging continues up to 80%.

5. NUMERICAL STUDIES

Figure 8 displays the combined microgrid including AC, DC, and DC resources, load, and load bus along with the main interface converter between both sides. The AC voltage is 600 V and the frequency is 60 Hz, while the DC voltage is equal to 400 V. In AC and DC, there are potential resources such as wind and PV. The line resistance and inductance between the buses are considered in AC. In this section, sustainability is analyzed on a combined network. Initially, stability analysis is performed on a hybrid network. AC and DC power output are 3 MW [22].

As mentioned, this study aims to survey if there is a combined network of AC/DC resources and loads that can provide their loads for each separate region. Meanwhile, both regions of this network are connected through a bidirectional interface converter. In addition, the system can operate in the network and islanded mode. These islands occur on any side. Eigenvalue analysis is widely used to evaluate dynamic stability in power systems. To find system eigenvalues, system operating points must be obtained by load distribution analysis or via time domain simulation. The operational points of the stable simulation mode are obtained through the MATLAB Simulink. Figure 9 indicates the diagram of the Eigenvalue of AC/DC microgrid. In addition, the eigenvalue of the AC/DC system is shown in Figures 10 and 11.

Higher droop values in AC microgrids are required to share the appropriate power between resources as well as to improve the system transient response. However, a higher droop in DC microgrid leads to increase power-sharing, voltage drop, and stability reduction. The main goal is to control and maintain the voltage stability and system frequency as fast as possible. The loads on both sides should be supplied with a stable voltage and frequency. In the islanded mode, the system stability should be studied when a fault occurs on the generation side or when the load suddenly changes. In case of reduction of production or increase of load, power exchange occurs in such a way that the network has the minimum voltage and frequency changes. Further, the stability impact on each side is reduced compared to the other side.

In this study, nonlinear control is used for stability analysis in AC/DC hybrid microgrid with bidirectional interface converter. To evaluate the performance of this model, comparisons between the performance of this model and the linear control method proposed by Dheer et al. [12] are presented, in different operating scenarios.

Some scenarios have been explored to evaluate the effectiveness of the proposed control system.

1) Combined microgrid equilibrium mode, where the load power of each side is less than the production power;
2) Changing load and power exchange from AC to DC and vice versa;

Separation of AC side from the DC side.

In the first scenario, the microgrid is initially operated in the islanded mode. In this case, the load power of AC and DC is equal to 2.5 and 1 MW, respectively. In the first second, the load power of each AC and DC side grows by 0.5 MW. The control system of each source raises its output power by changing the voltage on the DC side as well as the voltage and frequency on the AC side to augment the load. Since the generating power capacity of each side is equal to 3 MW and the load power to the AC and DC side has increased by 3 and 1.5 MW, respectively. The load power is supplied by the same side sources and will not pass through the power interface converter. In this state, the hybrid microgrid is normal and the independent control system of each source can boost production and supply load on each side.

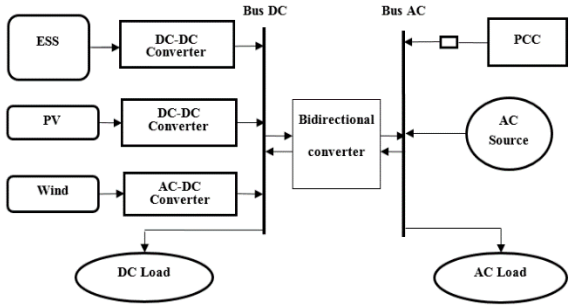

Figure 8. The diagram of AC/DC microgrid model

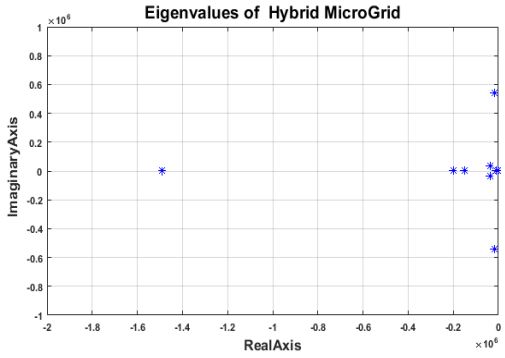

Figure 9. The eigenvalue of hybrid AC/DC microgrid

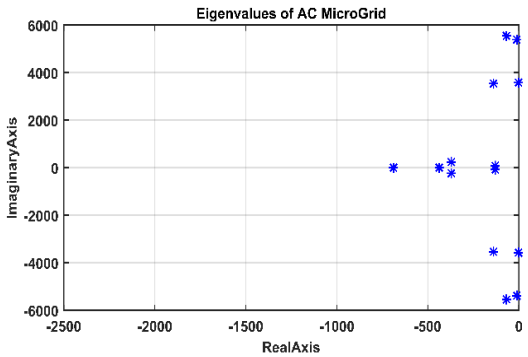

Figure 10. The eigenvalue of AC in the hybrid microgrid

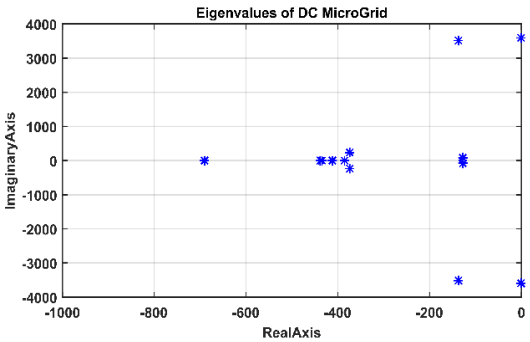

Figure 11. The eigenvalue of DC in the hybrid microgrid

For evaluation and better expression of the performance, the proposed independent nonlinear control method has been compared with the conventional linear control method. Figures 12 and 13 depict the AC and DC power, respectively. As displayed in the figure, the power oscillates in 1 s due to the increase in load and stabilizes in less than 0.2 s with the minimum oscillation. Figures 14 and 15 indicate the AC and DC voltages, respectively. The voltage fluctuations generated in 1 shave been controlled and it can be seen that the independent nonlinear control very well controlled the voltage fluctuations at the same time as the load changes. Figure 16 also reveals the frequency fluctuations per second. The power changes in the bidirectional converter in 1s are also shown in Figure 17. The power passing through the bidirectional converter in this case is zero. The comparison of the proposed method and conventional linear control suggests that the independent nonlinear

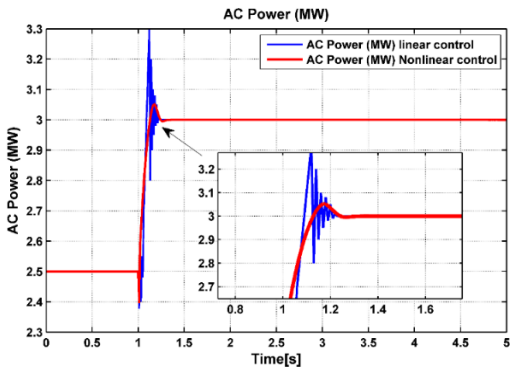

Figure 12. Production power by AC side sources

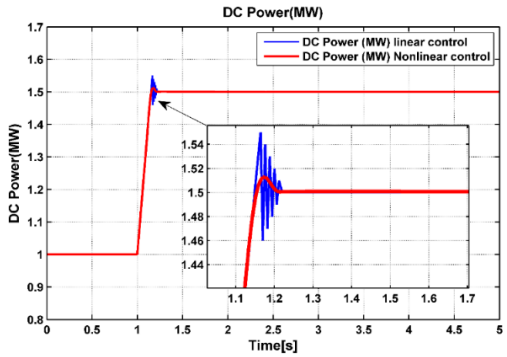

Figure 13. Production power by DC side sources

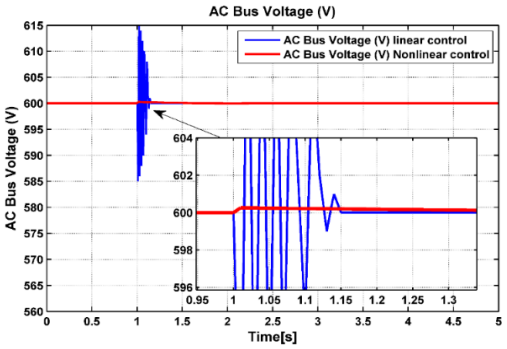

Figure 14. AC bus voltage during load changes

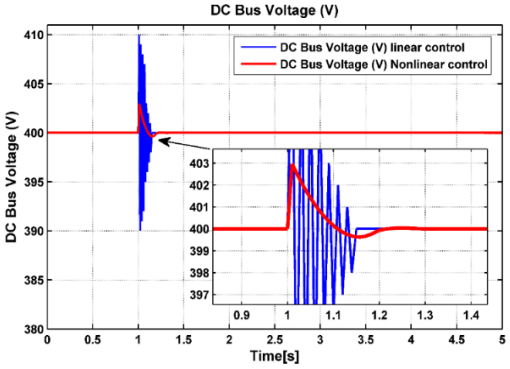

Figure 15. DC bus voltage during load changes

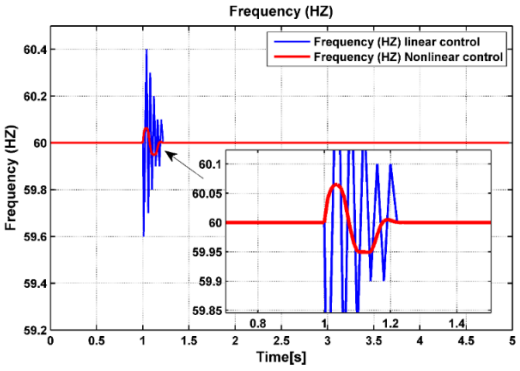

Figure 16. AC bus frequency during load changes

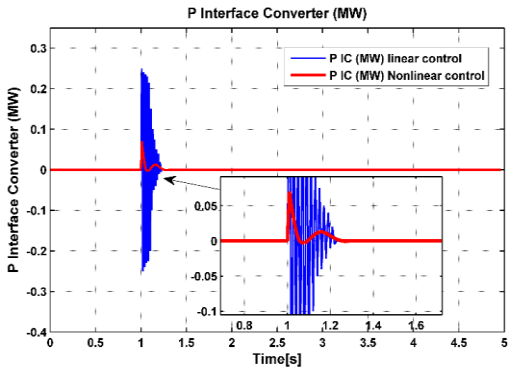

Figure 17. The power flow of the bidirectional converter

control system has followed the load changes within the shortest time and with the minimum fluctuations.

In the second scenario, to express the efficiency of the independent nonlinear control system and to control the bidirectional converter, the power exchange challenge from AC to DC and vice versa is examined. AC and DC side loads are 2.5 and 1 MW, respectively, and the system is in equilibrium. Initially, the DC side load power rises to 2 to 3.2 MW per second. Since the power capacity of each side is equal to 3 MW, the DC side required0.2 MW of power to supply the load. To this aim, the interface converter must transfer a power equivalent to 0.2 MW from AC to DC. The sources on the DC side try to supply the load at their maximum capacity. Figures 18 and 19 depict the AC and DC power output, respectively.

In 2s to supply power to the DC side, the output power of the AC side increases to 2.7 MW. Figure 20 illustrates the transfer power of the converter in rectifier mode. Also, the AC and DC voltage changes are shown in Figures 21 and 22. According to the comparison, the fluctuations due to power changes in the interface converter and DC and AC side are well controlled by the independent nonlinear control system; compared to conventional linear control, the combined microgrid system is stable with minimum time and oscillation.

In the next mode of the second scenario, the AC side power grows from 2.5 to 3.5 MW in 2s. DC microgrid

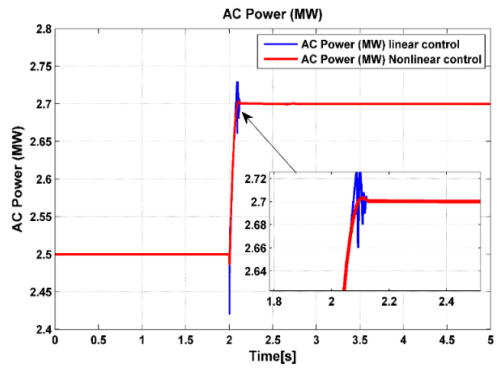

Figure 18. Production power by AC side sources

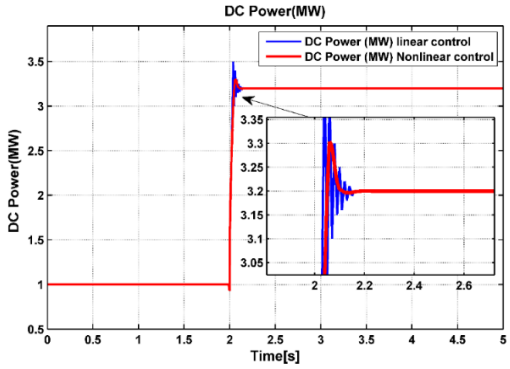

Figure 19. Production power by DC side sources

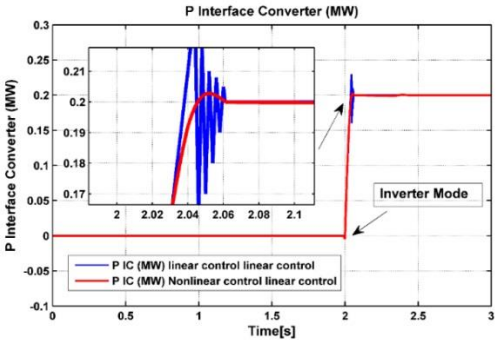

Figure 20. The power flow of the bidirectional converter

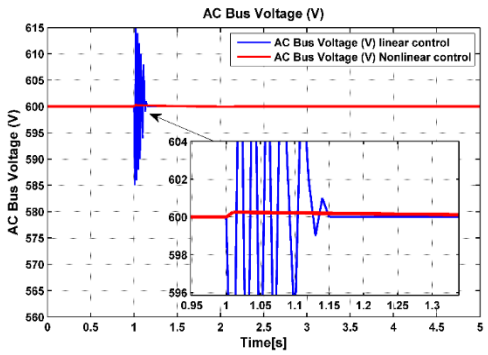

Figure 21. AC bus voltage during load changes

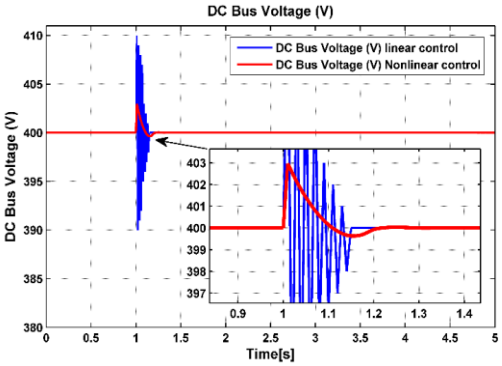

Figure 22. DC bus voltage during load changes

power is 1 MW. Since the load power required by the AC side is less than the output capacity of that side, the interface converter need to be able to transfer 0.5 MW from the DC side to the AC. Figures 23 and 24 show the power changes on the AC and DC sides, respectively. Also, the bidirectional converter operates in the inverter mode and transmits a power equivalent to 0.5 MW to AC (Figure 25). In addition, voltage changes on both sides are shown in Figures 26 and 27. Considering the precise performance of independent nonlinear control and its comparison with the conventional linear control method, it can be stated that changes and power exchange in each direction are handled by the proposed control system in the shortest time, which ensures system stability.

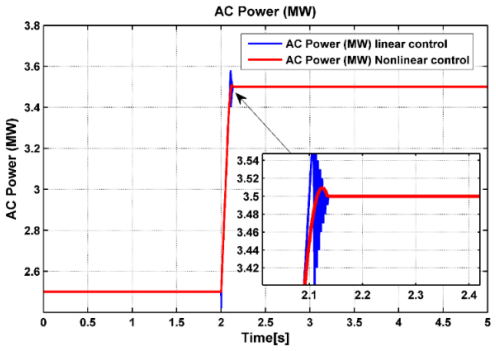

Figure 23. Production power by AC side sources

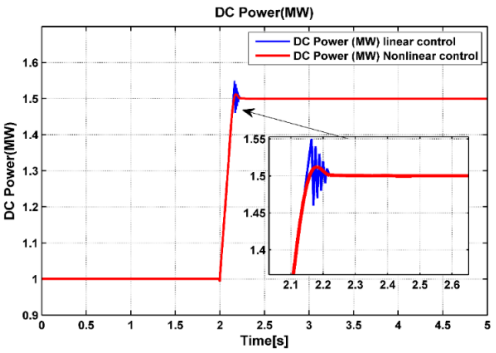

Figure 24. Production power by DC side sources

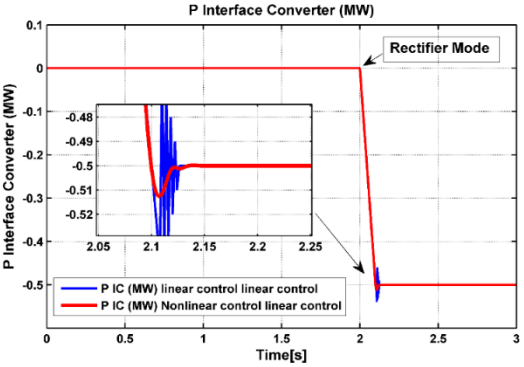

Figure 25. The power flow of the Bidirectional converter

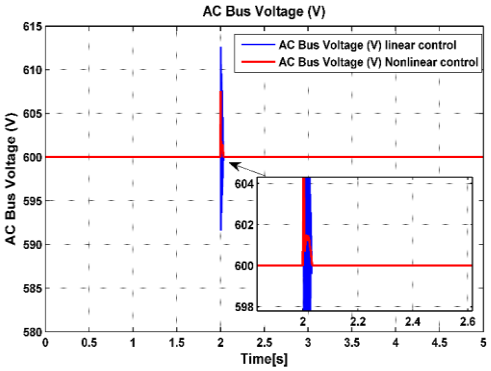

Figure 26. DC bus voltage during load changes

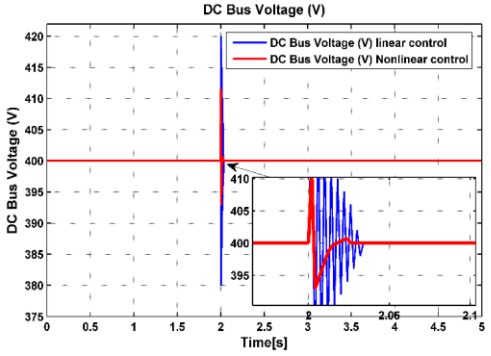

Figure 27. DC bus voltage during load changes

In the third scenario, the bidirectional converter is challenged. In 2s, due to repairs or faults in the system, the bidirectional converter is taken out of the circuit and then returned to the system in 3.5s. Figure 28 reveals the power changes in the bidirectional converter. In this case, it is assumed that the increase in load on each side is controlled and the necessary measures are taken to reduce the load. Figures 29 and 30 indicate the AC and DC voltage changes; while, Figure 31 depicts the frequency changes in 2 and 3.5s.

In this case, the major fluctuations will be on the voltage and frequency of the combined microgrid. This

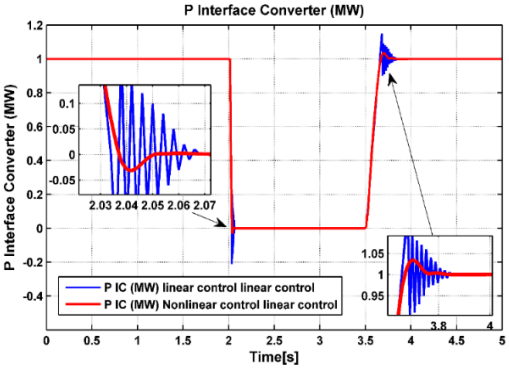

Figure 28. The power flow of the bidirectional converter

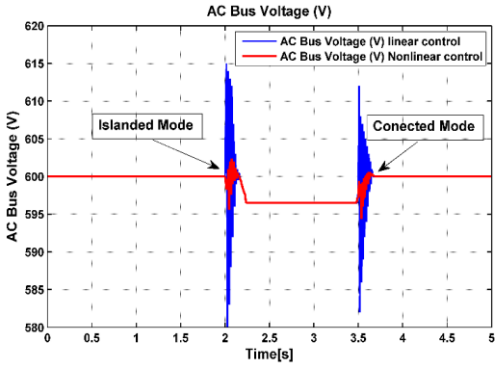

Figure 29. AC bus voltage during the islanded and reconnection mode

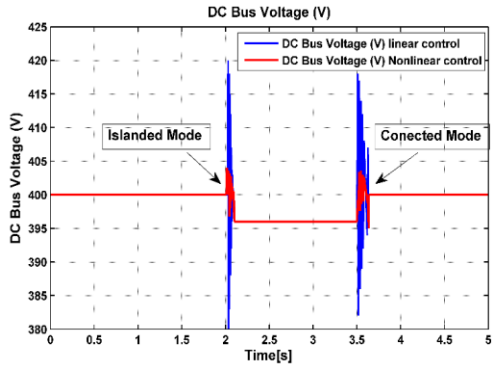

Figure 30. DC bus voltage during the islanded and reconnection mode

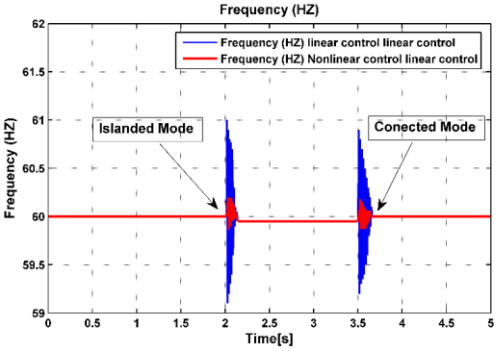

Figure 31. AC bus Frequency during the islanded and reconnection mode

is because the two parts are separated and the independent nonlinear control system must be able to supply the loads on each side as well as keep the system voltage plus frequency constant. by comparison, it can be seen that the independent nonlinear control system follows the changes very accurately. also, by controlling the power changes on both ac and dc sides by independent controllers, it ensures the stability of the voltage and frequency of the combined microgrid.

6. CONCLUSION

In this paper, a nonlinear controller was introduced to improve the stability of microgrids in islanded mode. In the proposed model, AC resources and loads on one side were related to DC resources and loads on the other side through a bidirectional AC/DC interface converter. Also, the hybrid microgrid would maintain its power balance in each part and use the other side for the power supply if there is unbalancing. In this model, each part, in addition to its load, could provide the other side load through a bidirectional interface converter. Accordingly, a nonlinear controller was used to properly stabilize the AC bus frequency and the DC bus voltage proportionate with the load changes on both sides. Also, the coordinated exchange and optimal regulation of control signals in this structure led to improve stability and in turn improved system performance. Here, the control systems existing for each source first increased the load deficiency and changed the system power with voltage and frequency variations while generating the maximum required power. Meanwhile, once changes are received by AC and DC buses on both sides of the converter, the control system would receive load changes, power shortages or faults and act accordingly. In such a system, a central converter was responsible for power exchange instead of using several converters. In addition, an energy storage system was used to improve the stability. With this proposed method, voltage and frequency fluctuations became stable during the first few cycles. What maintains stability in this network has been the correct exchange of power between two parts. This is performed by designing the bidirectional interface converter control system carefully and practically. This nonlinear control system ensures system stability.

7. REFERENCES

1. Armghan, H., Yang, M., Wang, M., Ali, N., Armghan, A.J.I.J.o.E.P. and Systems, E., "Nonlinear integral backstepping based control of a dc microgrid with renewable generation and energy storage systems", ***International Journal of Electrical Power & Energy Systems,*** Vol. 117, No., (2020), 105613, doi: 10.1016/j.ijepes.2019.105613.
2. Gundabathini, R., Pindoriya, N.M.J.E.P.C. and Systems, "Improved control strategy for bidirectional single phase ac-dc converter in hybrid ac/dc microgrid", ***Journal of Electrical Power Components Systystems,*** Vol. 45, No. 20, (2017), 2293-2303, doi: 10.1080/15325008.2017.1402970.
3. Pourbehzadi, M., Niknam, T., Aghaei, J., Mokryani, G., Shafie-khah, M., Catalão, J.P.J.I.J.o.E.P. and Systems, E., "Optimal operation of hybrid ac/dc microgrids under uncertainty of renewable energy resources: A comprehensive review", ***Electronic Power Energy System***, Vol. 109, No., (2019), 139-159, doi: 10.1016/j.ijepes.2019.01.025.
4. Jin, N., Hu, S., Gan, C. and Ling, Z.J.I.T.o.I.E., "Finite states model predictive control for fault-tolerant operation of a three-phase bidirectional ac/dc converter under unbalanced grid voltages", ***IEEE Transactions Industrial Electronics***, Vol. 65, No. 1, (2017), 819-829, doi: 10.1109/TIE.2017.2686342.
5. Issa, W., Al-Naemi, F., Konstantopoulos, G., Sharkh, S. and Abusara, M.J.E.P., "Stability analysis and control of a microgrid against circulating power between parallel inverters", ***Energy Procedia***, Vol. 157, No., (2019), 1061-1070, doi: 10.1016/j.egypro.2018.11.273.
6. Li, P., Yan, S., Yu, X. and Zhang, J., "The h∞ control method of bidirectional converter in hybrid ac/dc microgrid", in 2016 IEEE Power and Energy Society General Meeting (PESGM), IEEE. Vol., No., (2016), 1-5.
7. Dragičević, T., Lu, X., Vasquez, J.C. and Guerrero, J.M.J.I.t.o.p.e., "Dc microgrids—part ii: A review of power architectures, applications, and standardization issues", ***IEEE Transactions on Power Electronics,*** Vol. 31, No. 5, (2015), 3528-3549, doi: 10.1109/TPEL.2015.2464277.
8. Malik, S.M., Ai, X., Sun, Y., Zhengqi, C., Shupeng, Z.J.I.G., Transmission and Distribution, "Voltage and frequency control strategies of hybrid ac/dc microgrid: A review", ***IET Generation, Transmission & Distribution,*** Vol. 11, No. 2, (2017), 303-313, doi: 10.1049/iet-gtd.2016.0791.
9. Zubieta, L.E.J.I.E.M., "Are microgrids the future of energy?: Dc microgrids from concept to demonstration to deployment", ***IEEE Electrification Magazine,*** Vol. 4, No. 2, (2016), 37-44, doi: 10.1109/MELE.2016.2544238.
10. Han, H., Hou, X., Yang, J., Wu, J., Su, M. and Guerrero, J.M.J.I.T.o.S.G., "Review of power sharing control strategies for islanding operation of ac microgrids", ***IEEE Transactions on Smart Grid***, Vol. 7, No. 1, (2015), 200-215, doi: 10.1109/TSG.2015.2434849.
11. Hatziargyriou, N., "Microgrids: Architectures and control, John Wiley & Sons, (2014).
12. Dheer, D.K., Soni, N., Doolla, S.J.S.E., Grids and Networks, "Improvement of small signal stability margin and transient response in inverter-dominated microgrids", ***Sustainable Energy Grids and Networks***, Vol. 5, (2016), 135-147, doi: 10.1016/j.segan.2015.12.005.
13. Khorsandi, A., Ashourloo, M., Mokhtari, H., Iravani, R.J.I.G., Transmission and Distribution, "Automatic droop control for a low voltage dc microgrid", ***IET Generation, Transmission and Distribution,*** Vol. 10, No. 1, (2016), 41-47, doi: 10.1049/iet-gtd.2014.1228.
14. Tejwani, V.S. and Suthar, B.N., "Control strategy for utility interactive hybrid pv hydrogen system", in 2016 IEEE Power and Energy Society General Meeting (PESGM), IEEE. (2016), 1-5.
15. Yu, K., Ai, Q., Wang, S., Ni, J. and Lv, T.J.I.T.o.S.G., "Analysis and optimization of droop controller for microgrid system based on small-signal dynamic model", ***IEEE Transactions on Smart Grid***, Vol. 7, No. 2, (2015), 695-705, doi: 10.1109/TSG.2015.2501316.
16. Thale, S.S. and Agarwal, V.J.I.T.o.S.G., "Controller area network assisted grid synchronization of a microgrid with renewable energy sources and storage", ***IEEE Transactions on Smart Grid,*** Vol. 7, No. 3, (2015), 1442-1452, doi: 10.1109/TSG.2015.2453157.
17. Alnejaili, T., Drid, S., Mehdi, D., Chrifi-Alaoui, L., Belarbi, R., Hamdouni, A.J.E.C. and Management, "Dynamic control and advanced load management of a stand-alone hybrid renewable power system for remote housing", ***Energy Conversion and Management,*** Vol. 105, (2015), 377-392, doi: 10.1016/j.enconman.2015.07.080.
18. Dragičević, T., Guerrero, J.M., Vasquez, J.C. and Škrlec, D.J.I.T.o.p.E., "Supervisory control of an adaptive-droop regulated dc microgrid with battery management capability", ***IEEE Transactions on Power Electronics,*** Vol. 29, No. 2, (2013), 695-706, doi: 10.1109/TPEL.2013.2257857.

19. Abdullah, M.A., Yatim, A., Tan, C.W., Saidur, R.J.R. and reviews, s.e., "A review of maximum power point tracking algorithms for wind energy systems", ***Renewable and Sustainable Energy Reviews,*** Vol. 16, No. 5, (2012), 3220-3227, doi: 10.1016/j.rser.2012.02.016.

20. Du, C., Agneholm, E. and Olsson, G.J.I.T.o.P.D., "Comparison of different frequency controllers for a vsc-hvdc supplied system", ***Transactions on Power Transmission & Distribution***, Vol. 23, No. 4, (2008), 2224-2232, doi: 10.1109/tpwrd.2008.921130.

21. Ruan, S.-Y., Li, G.-J., Peng, L., Sun, Y.-Z., Lie, T.J.I.J.o.E.P. and Systems, E., "A nonlinear control for enhancing hvdc light transmission system stability", ***International Journal of Electrical Power & Energy Systems,*** Vol. 29, No. 7, (2007), 565-570, doi: doi: 10.1016/j.ijepes.2007.01.008.

22. Yang, P., Xia, Y., Yu, M., Wei, W. and Peng, Y.J.I.T.o.I.E., "A decentralized coordination control method for parallel bidirectional power converters in a hybrid ac–dc microgrid", ***IEEE Transactions Industrial Electronics***, Vol. 65, No. 8, (2017), 6217-6228, doi: 10.1109/TIE.2017.2786200.

Persian Abstract

چکیده

این مطالعه، ساختار جدیدی مبتنی بر کنترل‌کننده غیرخطی برای کنترل و تجزیه و تحلیل ثبات ریزشبکه‌های ترکیبی ارائه می‌دهد. در مدل پیشنهادی، منابع و بارهای AC و DC در دو طرف مختلف قرار دارند. علاوه بر این ، یک مبدل رابط دوطرفه AC / DC برای تأمین بار توسط منابع AC / DC استفاده شده است. تولیدات AC / DC در هر دو طرف مبدل وجود دارد و هر طرف می‌تواند بار طرف دیگر را از طریق مبدل رابط دو طرفه تأمین کند. همچنین، یک سیستم ذخیره انرژی برای پایداری سیستم در سمت DC استفاده شده است. کنترل‌کننده غیرخطی ریزشبکه برای تنظیم صحیح فرکانس سمت باس AC و ولتاژ سمت باس DC طراحی شده است. در این ساختار، تبادل هماهنگ و بهینه توان همراه با تنظیم دقیق سیگنال‌های کنترل منجر به بهبود پایداری می‌شود. بنابراین، عملکرد سیستم بهبود می‌یابد. نتایج نشان می‌دهد که مدل پیشنهادی برای کاهش نوسانات و بهبود پایداری سیستم کارآمد است.